Scheme for a compact cold-atom clock based on diffuse laser cooling in a cylindrical cavity

Peng Liu, Yanling Meng, Jinyin Wan, Xiumei Wang, Yaning Wang, Ling Xiao, Huadong Cheng,* and Liang Liu†
Key Laboratory of Quantum Optics and Center of Cold Atom Physics, Shanghai Institute of Optics and Fine Mechanics, Chinese Academy of Sciences, Shanghai 201800, China
(Received 25 September 2015; published 3 December 2015)

We present a scheme for a compact rubidium cold-atom clock which performs diffuse light cooling, microwave interrogation, and detection of the clock signal in a cylindrical microwave cavity. The diffuse light is produced by laser light reflection at the inner surface of the microwave cavity. The pattern of the injected laser beams is specially designed to accumulate the majority of the cold atoms in the center of the microwave cavity. Microwave interrogation of the cold atoms in the cavity leads to Ramsey fringes, which have a linewidth of 24.5 Hz with a contrast of 95.6% when the free evolution time is 20 ms. Recently, a frequency stability of $7.3 \times 10^{-13}\ \tau^{-1/2}$ has been achieved. The scheme of this physical package can largely reduce the cold-atom clock complexity and increase clock performance.

DOI: 10.1103/PhysRevA.92.062101 PACS number(s): 06.20.−f, 37.10.De, 42.50.Ct, 42.62.Fi

I. INTRODUCTION

Over the past 20 years, impressive progress has been made for atomic clocks thanks to the application of laser and cold-atom techniques. The laser-pumped rubidium vapor-cell clock has been demonstrated by replacing the lamp with a compact frequency-stabilized laser [1]. Godone *et al.* developed a clock scheme known as a pulsed optically pumped (POP) clock in a vapor cell that uses a diode laser for optical pumping and the Ramsey technique for interrogating atoms [2–4]. In this POP scheme, the light shift can be greatly reduced.

With the development of the cold-atom technique, the vapor cell of the POP scheme can be replaced by cold atoms, which have less temperature sensitivity and much longer coherent times than the vapor cell; thus, the cold atoms could improve the clock performance. Müller *et al.* have cooled and interrogated cesium atoms inside a cylindrical stainless steel cavity by applying a magneto-optical trap (MOT) [5]. However, the strong magnetic field of the MOT will lead to magnetization of the stainless steel over long-term clock operations. Consequently, the clock performance will be reduced. Moreover, the six windows on the cavity required by MOT also affect the inner microwave field mode.

A more attractive method to cool atoms for a POP clock is diffuse light cooling [6–8]. Typically, diffuse light is generated inside a sphere by the diffuse multireflection of injected lasers on the inner surface of the sphere. Diffuse light cooling does not require fine adjustment of lasers and can efficiently cool atoms with zero or weak magnetic fields. Thus this scheme is very robust. The cesium atom clock named HORACE, which uses a three-dimensional (3D) isotropic light cooling configuration has achieved a relative frequency stability of $2.2 \times 10^{-13}\ \tau^{-1/2}$ and 3×10^{-15} at the integrating time of 10^4 s [9,10]. Better performance is expected in microgravity environments which makes HORACE a strong candidate for an onboard satellite clock. We previously developed a similar clock with rubidium atoms [11].

In this paper, we describe the development of a compact cold-atom clock based on diffuse light cooling in a cylindrical microwave cavity. Unlike HORACE, which uses a spherical cavity, the cylindrical cavity used in our experiment enables both diffuse light cooling and microwave interrogation with cold atoms [12–14]. Furthermore, a technique for controlling the distribution of the cold-atom cloud inside the cavity is applied. With this technique, more atoms can be accumulated at the center of the cavity [14,15].

This paper is organized as follows. Section II gives a detailed description of the optical and physical package. Section III describes the time sequence of the experiment and discusses the frequency stability of the atomic clock. Section IV evaluates the factors that affect the frequency stability of the atomic clock. Finally, Sec. V concludes the results and discusses its further applications.

II. RUBIDIUM-ATOM CLOCK CONFIGURATION

The physical package is shown in Fig. 1. The microwave cavity is fabricated with oxygen-free copper, and the inner surface is coated with silver to increase the diffuse reflectance at 780 nm (96.6%). Four holes with diameter of 3 mm are centrosymmetrically distributed in the undersurface of the cavity for injecting lasers vertically to the microwave cavity. Four multimode fibers are used to transport the cooling, repumping, and pumping lights to the physical package [14]. The light intensity imbalance of these four fibers is less than 0.25%. For microwave interrogation, we use a microwave coupling loop horizontally placed in the middle of the internal cylinder in order to obtain a large uniform area of microwave field. The microwave cavity operates at the TE011 mode with a quality factor about 11000. We fix the microwave cavity in a vacuum chamber where the vacuum is maintained at about 2.3×10^{-10} Torr by ion pumps. The magnetic coils producing constant longitudinal magnetic fields (12 mG) are intertwined around the vacuum chamber. The vacuum chamber and magnetic coils are covered by five layers of magnetic shielding, which can reduce the internal residual stray magnetic field to less than 1 nT. Moreover, heating coils surround the first layer for the temperature control loop.

*chenghd@siom.ac.cn
†liang.liu@siom.ac.cn

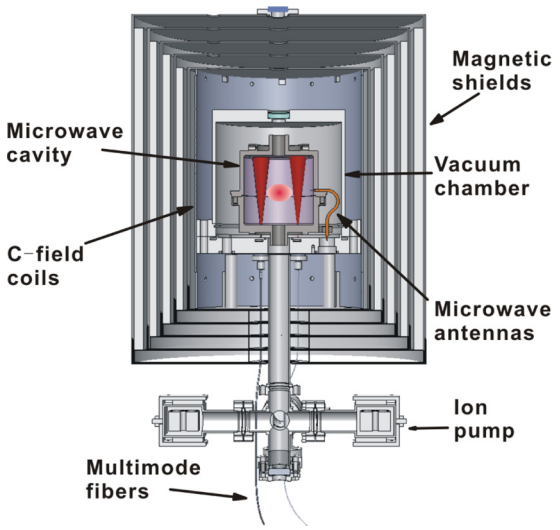

FIG. 1. (Color online) Physical schematic of the atomic clock. The cold atoms are captured in the central region of the microwave cavity, and the cold atom density is about four times larger than that of the previous cooling structure [11].

Figure 2 shows the schematic of the light path. Atoms are cooled and manipulated in the center of the cavity [15] with an extended-cavity diode laser (ECDL) as the source of cooling light which is red detuned by about 22.8 MHz to the transition $5\,^2S_{1/2},|F=2\rangle \rightarrow 5\,^2P_{3/2},|F'=3\rangle$ of the ^{87}Rb D_2 line. A second ECDL which is locked to the transition $5\,^2S_{1/2},|F=1\rangle \rightarrow 5\,^2P_{3/2},|F'=2\rangle$, provides the repumping laser. In the quantum state preparation stage, a short pulse of pumping light tuned to the transition of $5\,^2S_{1/2},|F=2\rangle \rightarrow 5\,^2P_{3/2},|F'=1\rangle$ is applied. The probe laser emits from the third ECDL with a linewidth of about 100 kHz. The probe laser intensity is stabilized [the intensity fluctuation is detected by a photodetector (PD2) in Fig. 2], and the frequency is shifted to be almost resonant to the transition $5\,^2S_{1/2},|F=2\rangle \rightarrow 5\,^2P_{3/2},|F'=3\rangle$. The diameter of the probe beam is extended to 6 mm and collimated by two lenses before being injected into the physical package. Because the acousto-optic modulator (AOM) is not an ideal optical switch and residual light will decrease the signal-to-noise ratio ($R_{\rm SN}$) of the clock signal and lead to light shift, four low-vibration mechanical shutters are used for switching off the cooling, pumping, repumping, and probe beams.

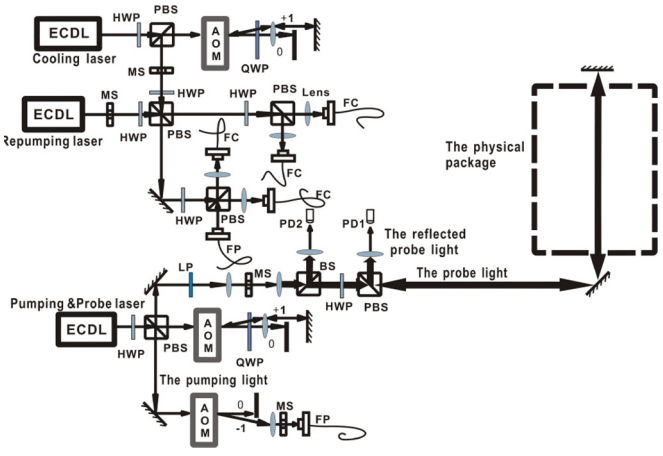

FIG. 2. (Color online) Schematic of the light path, where ECDL: extended-cavity diode laser, QWP: quarter wave plate, HWP: half wave plate, PBS: polarizing beam splitter, BS: beam splitter, LP: linear polarizer, FP: fibers for pumping light, FC: fibers for cooling light, PD1: photodetector for detecting clock signals, PD2: photodetector for intensity stabilization of the probe light, and MS: mechanical shutter.

III. TIME SEQUENCE OF THE CLOCK OPERATION

Typically, the Allan deviation which is used to evaluate the frequency stability of an atomic clock can be written as [16]

$$\sigma_y(\tau) = \frac{1}{\pi}\frac{\Delta\nu}{\nu_0}\frac{1}{C}\frac{1}{R_{\rm SN}}\sqrt{\frac{T_c}{\tau}}, \quad (1)$$

where C is the contrast of the Ramsey fringes, $\Delta\nu$ is the linewidth of the Ramsey fringes, and τ is the integrating time. For the integrating sphere atom clock, the free evolution time T_f for microwave interrogation is primarily limited by the free-falling process due to the gravity. Considering the size of the system, the maximum free-evolution time on Earth is about 50 ms. According to the relationship $\Delta\nu \sim 1/2T_f$, longer T_f means smaller $\Delta\nu$; meanwhile, the $R_{\rm SN}$ and contrast of the Ramsey fringes will decrease as T_f increases. Thus, we need to optimize the laser parameters and the time sequence for operating the atom clock. To ensure the microwave pulse can be used to realize the largest inversion of the atomic number between two $m_F = 0$ states of the ground states, the Rabi oscillation of the cold atoms needs to be determined to find the suitable microwave power. Figure 3 shows the Rabi oscillation for the microwave pulse duration of 6 ms by scanning the microwave power. The first peak in Fig. 3 corresponds to $\Omega t_m \approx \pi/2$, where Ω is the Rabi frequency and $t_m = 3$ ms.

Generally, as shown in Fig. 4, the time sequence of a cold-atom clock operation includes four stages: cooling of atoms, optical pumping, microwave interrogation, and detection of

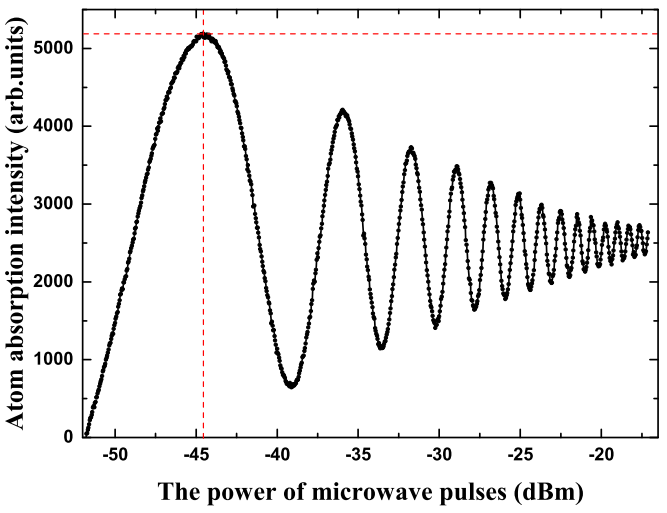

FIG. 3. (Color online) Rabi oscillation with the microwave pulse duration of 6 ms.

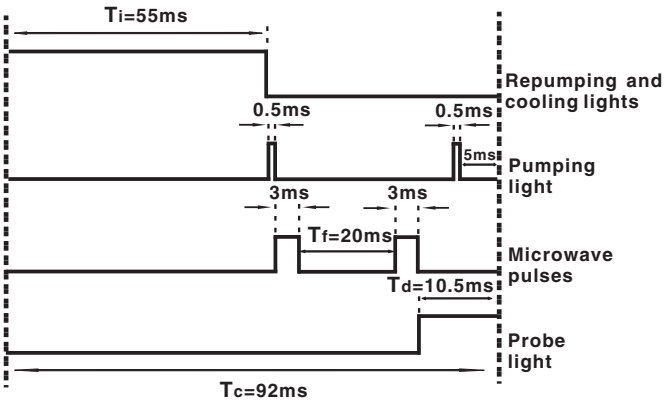

FIG. 4. Time sequence of the atomic clock. The cycle time T_c is 92 ms. The isotropic laser cooling stage T_i lasts 55 ms and the free evolution time T_f is 20 ms.

the clock signal. The 3D isotropic laser cooling lasts 55 ms during which at least 2.4×10^8 atoms are cooled and accumulated in the central region of the microwave cavity. After the first 0.5-ms optical pumping pulse, atoms are pumped into the $5\,^2S_{1/2}|F = 1\rangle$ state. Then, two 3-ms microwave pulses separated by 20-ms free evolution time are utilized for the Ramsey interrogation. The population of the atoms at the $5\,^2S_{1/2}|F = 2, m_F = 0\rangle$ state is detected by using a probe beam which is vertical and retroreflected in the axis of the cylinder cavity. The probe beam lasts 10.5 ms, and its intensity is 2.0 μW. There is a second 0.5-ms optical pumping pulse in the detection window for clearing out the cold atoms on $|F = 2, m_F = 0\rangle$ and the transmission of probe light after the second optical pumping pulse is also recorded. Thus, the absorption of cold atoms populated on $|F = 2, m_F = 0\rangle$ is the difference between the probe transmission signals recorded before and after the second optical pumping pulse.

Figure 5 shows the Ramsey fringes with $T_f = 20$ and 30 ms. As T_f increases, the linewidth of the central fringe changes

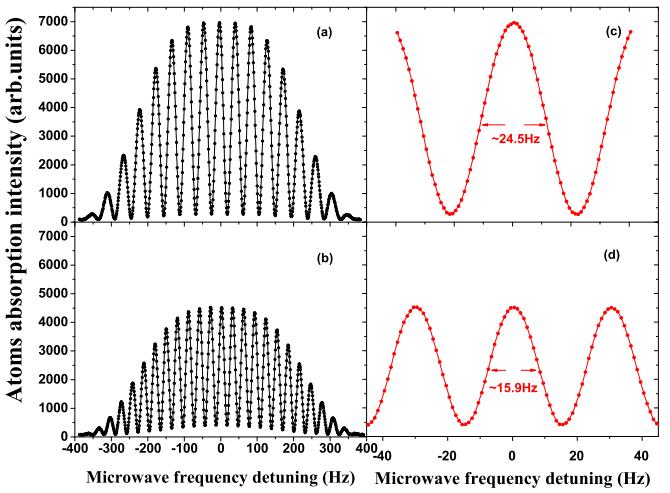

FIG. 5. (Color online) Ramsey fringes with a single measurement. The free evolution time (a) T_f =20 ms and (b) T_f=30 ms, where (c) shows the central fringes of (a), and (d) shows the central fringes of (b).

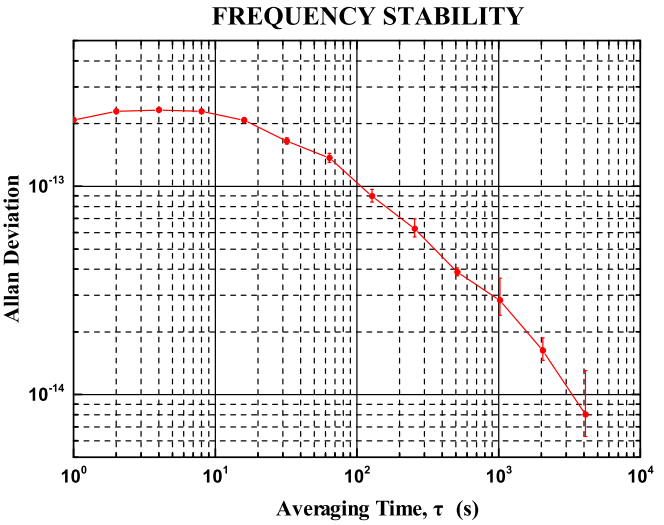

FIG. 6. (Color online) Allan deviation of the cold-atom clock by comparison with the H maser.

from 24.5 to 15.9 Hz, and the R_{SN} decreases from about 400 to 260. This is a tradeoff between large R_{SN} and narrow linewidth.

IV. ATOMIC CLOCK PERFORMANCE AND NOISE ESTIMATION

The error signal, which generates feedback for the local oscillator (LO), originates from the frequency-hopping detection of the clock transition at the FWHM of the central fringe, and the LO, which is the reference source of the microwave frequency synthesizer chain, is locked to the central fringe. The relative frequency stability is measured by comparing the LO frequency output with a hydrogen maser. A recent result is shown in Fig. 6. The frequency stability of 1.6×10^{-14} is reached after integrating for 2000 s.

The main limitations for the short-term frequency stability of the clock are the atomic shot noise, the intensity and frequency fluctuation of the probe laser (AM and FM), electronic noise, and the LO phase noise (Dick effect). In each cycle, according to the absorption signal, the number of cold atoms detected by the probe light can be estimated with the equation given by [17]

$$N = \frac{\pi r^2}{\sigma_0}\left[\frac{I_0 - I_t}{I_s} + \left(\frac{4\delta^2}{\Gamma^2} + 1\right)\ln\left(\frac{I_0}{I_t}\right)\right], \tag{2}$$

Here r is the radius of the probe beam, and δ is the detuning from atomic resonance. The probe light intensity before and after going through the physical package is given by I_0 and I_t, respectively. Moreover, Γ is the natural linewidth of the transition, σ_0 is the resonant cross-sectional area, and I_s is the on-resonance saturation intensity. These variables obey the following relationship [18]:

$$\sigma_0 = \frac{h\nu\Gamma}{2I_s}, \tag{3}$$

$$I_s = \frac{c\varepsilon_0 h^2\Gamma^2}{16\pi^2|\hat{\varepsilon}\cdot\vec{d}|^2}, \tag{4}$$

TABLE I. Noise budget of the system and instabilities of these noise sources.

Noise sources	Instability
AM and FM noises of the probe laser	$4.5 \times 10^{-13}\ \tau^{-1/2}$
Atomic shot noise	$4.7 \times 10^{-13}\ \tau^{-1/2}$
Electronic noise	$1.8 \times 10^{-13}\ \tau^{-1/2}$
Local oscillator phase noise	$2.7 \times 10^{-13}\ \tau^{-1/2}$
Total	$7.3 \times 10^{-13}\ \tau^{-1/2}$

Here ν is the frequency of the probe light, ε_0 is the free space permittivity, and h is the Plank constant. Moreover, $\hat{\varepsilon}$ is the unit polarization vector of the light field and $\vec{d}$ is the atomic dipole moment. Substituting Eqs. (3) and (4) into Eq. (2), we find that the number of cold atoms detected in each cycle is about 4.7×10^7 and about 8.5% of these atoms $N_a \approx 4.0 \times 10^6$ experience the "0-0" transition. Therefore, the corresponding atomic shot noise ($\sigma_{N_a} \sim 1/\sqrt{N_a}$) can be estimated as shown in Table I. Because the microwave interrogation process is not continuous and there is "dead time" in each cycle, the phase noises from LO and the frequency synthesizer will degrade the atomic clock performance. Here, the limit of the Dick effect with the commercial oscillator is about 2.7×10^{-13} on the condition that $S_y(f) = 10^{-29} f^2 + 1.3 \times 10^{-27} f + 1.3 \times 10^{-26}$. Table I gives the noise budget of the cold-atom clock.

The cavity pulling effect could be the primary contribution to the long-term frequency stability because it depends on the fluctuation of the cold-atom number and the cavity detuning from temperature fluctuation. In addition, microwave power fluctuations are also transferred to the clock transition through cavity pulling [19]. The long-term stability may be improved by decreasing the quality factor of the cavity and increasing the temperature stability of the system.

V. CONCLUSION

We report a compact cold-atom clock scheme that integrates all operation stages in a cylindrical microwave cavity. The use of diffuse laser cooling can simplify the structure and increase the reliability of the system because of its insensitivity to the laser polarization and alignment. The frequency stabilities of $7.3 \times 10^{-13}\ \tau^{-1/2}$ and 1.6×10^{-14} after integrating 2000 s are achieved. We believe that the frequency stability will be further improved after resolving these technical problems. Furthermore, its all-metal framework and better frequency stability in microgravity environments make it an excellent option for space applications. In addition, this scheme of a physical package can also be operated as a kind of high-efficiency precooling equipment for other physical experiments that require further steps of cooling.

ACKNOWLEDGMENTS

This work was supported by the National High Technology Research and Development Program of China (Grant No. 2012AA120702).

[1] C. Affolderbach, F. Droz, and G. Mileti, IEEE Trans. Instrum. Meas. **55**, 429 (2006).
[2] A. Godone, S. Micalizio, C. Calosso, and F. Levi, IEEE Trans. Ultrason. Ferroelectr. Freq. Control **53**, 525 (2006).
[3] A. Godone, S. Micalizio, F. Levi, and C. Calosso, Phys. Rev. A **74**, 043401 (2006).
[4] S. Micalizio, C. Calosso, A. Godone, and F. Levi, Metrologia **49**, 425 (2012).
[5] S. T. Müller, D. V. Magalhaes, R. F. Alves, and V. S. Bagnato, J. Opt. Soc. Am. B **28**, 2592 (2011).
[6] E. Guillot, P. E. Pottie, and N. Dimarcq, Opt. Lett. **26**, 1639 (2001).
[7] H. D. Cheng, W. Z. Zhang, H. Y. Ma, L. Liu, and Y. Z. Wang, Phys. Rev. A **79**, 023407 (2009).
[8] W. Z. Zhang, H. D. Cheng, L. Liu, and Y. Z. Wang, Phys. Rev. A **79**, 053804 (2009).
[9] F. X. Esnault, D. Holleville, N. Rossetto, S. Guerandel, and N. Dimarcq, Phys. Rev. A **82**, 033436 (2010).
[10] F. X. Esnault, N. Rossetto, D. Holleville, J. Delporte, and N. Dimarcq, Adv. Space Res. **47**, 854 (2011).
[11] B. C. Zheng, H. D. Cheng, Y. L. Meng, L. Xiao, J. Y. Wan, and L. Liu, Chin. Phys. Lett. **30**, 123701 (2013).
[12] Y. L. Meng, Y. C. Gao, B. C. Zheng, P. Liu, J. Y. Wan, L. Xiao, X. M. Wang, H. D. Cheng, and L. Liu, Chin. J. Lasers **41**, 0918001 (2014).
[13] Y. L. Meng, B. C. Zheng, P. Liu, J. Y. Wan, L. Xiao, X. M. Wang, Y. C. Gao, H. D. Cheng, and L. Liu, Acta Optica Sinica **34**, 0902001 (2014).
[14] Y. L. Meng, H. D. Cheng, B. C. Zheng, X. C. Wang, L. Xiao, and L. Liu, Chin. Phys. Lett. **30**, 063701 (2013).
[15] Y. L. Meng, H. D. Cheng, P. Liu, B. C. Zheng, L. Xiao, J. Y. Wan, X. M. Wang, and L. Liu, Phys. Lett. A **378**, 2034 (2014).
[16] J. Vanier and C. Audoin, *The Quantum Physics of Atomic Frequency Standards* (IOP, Bristol, U.K., 1989).
[17] G. D. McDonald, Detecting Atomic Shot Noise on Ultra-cold Atom Clouds, Honours thesis, Australian National University, 2009.
[18] D. A. Steck, Quantum and atom optics, available online at http://atomoptics-nas.uoregon.edu/~dsteck/teaching/.
[19] S. Micalizio, A. Godone, F. Levi, and C. Calosso, IEEE Trans. Ultrason. Ferroelectr. Freq. Control **57**, 1524 (2010).